Solar-assisted efficient cleanup of high-viscosity oil spills using magnetic porous biochar

Guanjie Zeng, Xiaozhong Huang, Jianling Yue, Benhui Fan, Yu Liu, Xiu-Zhi Tang

Solar-assisted efficient cleanup of high-viscosity oil spills using magnetic porous biochar

Guanjie Zeng[a], Xiaozhong Huang[b], Jianling Yue[b], Benhui Fan[c], Yu Liu[b], Xiu-Zhi Tang[d*]

a. School of Physics and Electronics, Central South University, Changsha, 410083, China.

b. Powder metallurgy research institute, Central South University, Changsha, 410083, China.

c. Equipe Recherche ENDSUM, Cerema, Les Ponts de Cé, 49136, France.

d. Research Institute of Aerospace Technology, Central South University, Changsha, 410083, China.

* Corresponding Author.

* Corresponding Author. Tel/Fax: 0731-88837927. E-mail: xztang@csu.edu.cn (Xiu-Zhi Tang)

Abstract: Efficient cleanup of oil spills is still a global challenge due to the high viscosity of crude oil and complicated topographic features. Herein, magnetic porous carbon powders (MPCs) with photothermal effect prepared at a $Fe(NO_3)_3$: bamboo mass ratio was 1/1 carbonized at 700 ºC. After modifying with the n-octadecylamine, the oleophilic MPCs exhibited rapid and selective absorption of different oils from polluted water, with an optimal absorption capacity of 3.2–8.1 g/g. Since oil's viscosity is highly temperature-sensitive, MPCs with photothermal characteristics offer apparent advantages in absorbing high viscosity oil. Moreover, due to the incorporation of magnetic components, powder-like MPCs can be conveyed to a specified oil pollution spot (including gaps or cracks) conveniently and collected through a remote magnetic field. This work demonstrates a simple and low-cost way of designing and producing oil/water separation materials, particularly floating high-viscosity oil recovery.

Keywords: High viscosity; Oil spill; Photothermal effect; Magnetic biochar; Oil/water separation

Introduction

The oil spill caused by offshore oil extraction or transportation causes enormous ecological disasters for the marine biosphere and the entire ecosphere of the earth [1-5]. The spilt oils will cover the water, block light and oxygen from reaching the deep ocean, and destroy marine life. Therefore, several cleanup solutions, including automated collection, biological breakdown, controlled burning, and chemical dispersants, have been proposed for oil spills [6-10]. Nonetheless, the implementation of these solutions has been hampered by a number of problems, including hazardous production, slow degradation, secondary pollution, etc. Consequently, it is essential to utilize more environmentally friendly methods for cleaning up the oil spill.

Using sorbent to recover oil from water is the most practical and effective method due to its minimal impact on the natural environment [11-13]. Porous materials have been regarded as effective absorbents, particularly oleophilic porous absorbents that can extract oil from water efficiently. Numerous materials, such as carbon-based aerogels, polymer sponges, and silica aerogels, have been produced based on this concept [14-16]. Upon application of these materials, several variables that influence their sorption ability must be considered. One parameter that impacts the separation speed and efficiency is the absorbent's shape. In the ocean, oil typically exists as emulsified droplets. Inadequate contact with the porous absorbent will significantly reduce separation efficiency [17, 18]. Therefore, a block-shaped absorbent is less effective due to its vast size, which results in inadequate interaction with the oil in the complicated topography[19, 20]. Alternatively, powder-like substances with a high specific surface area can produce successful oil-water separation in certain circumstances due to their sufficient interaction with tiny oil droplets [21-23]. In addition, by incorporating magnetic components into the powder absorbents, it is possible to achieve quick oil recycling by applying an external magnetic field and easily entering cracks or gaps.

Besides the influence of the absorbent's shape, the viscosity of the oil is also an essential component that influences the adsorption efficiency. The viscosity of crude oil is

usually as high as 10^3~10^5 mPa·s, which makes it difficult to be absorbed into porous absorbents[24]. Numerous studies have been conducted to reduce the viscosity of crude oil and boost the absorbent's adsorption efficiency. Yu et al. demonstrated a graphene-coated sponge, which could clean viscous crude oil as the Joule heating effect was stimulated [25]. Their following work also reported a ferrimagnetic sponge with a magnetocaloric effect [26]. When the sponge was exposed to an alternating current magnetic field, the viscosity of the crude oil around the sponge decreased due to magnetic heating. However, the electric-consumption activation method for the Joule heat effect is uneconomical in the maritime environment.

Solar energy is more environmentally benign and adaptable to the ocean than electrical energy. In this field, developing photothermal absorbents that can rapidly convert solar energy to thermal energy will be advantageous [27-29]. Due to its broad-spectrum solar light absorption, ultralow density, high porosity, high lipophilicity, environmental safety, and physical/chemical stability, carbon-based materials, such as graphene, carbon nanotubes, and carbon fiber, have been widely studied [30-33]. However, these carbon nanoparticles are too costly for widespread use. Considering that the carbon source from biomass is abundant, renewable, biodegradable, and low-cost, there has been an increased focus on developing carbon-based materials from renewable resources, such as agricultural wastes and natural products [34-36]. However, few investigations have been conducted to creat magnetic and photothermal powder absorbents generated from sustainable natural resources for viscous oil treatment.

In this work, the agricultural waste bamboo powders and ferric nitrate were employed as a carbon source to manufacture magnetic porous carbon powders (MPCs) with desirable photothermal performance for viscous oil cleanup. We utilized a method inspired by mussel to graft nonpolar n-octadecylamine (ODA) onto MPCs using polydopamine (PDA). The hydrophobic product ODA-MPCs developed displayed a high capacity for oil absorption and a high tolerance for acidic, alkaline, and hypersaline conditions. Meanwhile, the MPCs successfully generated heat effects under solar

radiation, significantly increasing the oil's fluidity. When the oil's viscosity reaches 5000 mPa·s, its absorption capacity reaches its maximum of 8.1 g/g.

Experiments

Materials

Bamboo powders were obtained from a local wood factory (Changsha, China). 3-hydroxytryptamine hydrochloride (dopamine), methylbenzene, n-hexane and tris-(hydroxymethyl) aminomethane (TRIS, 99%, a buffer agent) were purchased from Sigma-Aldrich Co., Ltd (Shanghai, China). n-octadecylamine (ODA) and ethanol were purchased from Aladdin Reagent Co., Ltd (Shanghai, China). The peanut oil was purchased from the local grocery store. Dow Chemical Company supplied silicon oil (Michigan, America). We purchased tetrahydrofuran and ethyl acetate from Sinopharm Chemical Reagent Co., Ltd. (Shanghai, China). The procurement of conduction oil from MOJIEZUO Co., Ltd. (Shanghai, China). Liaohe Oilfield was the source of petroleum (Panjin, China). All chemical reagents and solvents were used as received without further purification.

Preparation of magnetic porous carbons

The bamboo powders were firstly immersed in ferric nitrate solution at 90 °C under constant stirring until the complete evaporation of visible water. After being dried at 100 °C for 6 h, the red powders were transferred to a tube furnace and carbonized at high temperatures for 2 h with 100 mL min^{-1} of Ar flow protection. The pyrolyzed black powders are washed with *n*-hexane three times and dried at 60 °C for 2 h. The obtained MPCs were labeled as C-1, C-2, C-3, C-4 and C-5, respectively, according to different fabricated preparation conditions. (**Table 1**).

Table 1. Formulas and preparation conditions for MPCs

MPCs	Mass ratio ($Fe(NO_3)_3$:bamboo)	sintering temperature
C-1	1:2	600
C-2	1:1	600
C-3	2:1	600
C-4	1:1	700

C-5	1:1	800

Oleophilic modification of porous carbon

As-prepared MPCs were dispersed in 100 mL buffer solution (10 mM, pH=8.5) followed by adding 270 mg dopamine. After a bath sonication of 10 min, the suspension was stirred at room temperature for 24 h. The PDA-coated MPCs were then collected via solid-liquid separation and a water-washing treatment before being dried in a vacuum oven at 50 °C for 24 h. Subsequently, PDA-coated MPCs were redispersed in 100 mL ethanol containing 2 mmol ODA for oleophilic modification. After stirring for 24 hours, the collected solids were filtrated and rinsed with ethanol to remove unreacted ODA. Finally, the modification product MPCs-ODA was dried at 50 °C under a vacuum for 24 h.

Material characterizations

The morphologies of all samples were observed by scanning electron microscope (SEM). X-ray diffraction (XRD) measurements were carried out on an X-ray powder diffractometer (Bruker D8 Advance, Germany). N_2 adsorption/desorption isotherms were measured using a surface area and porosimetry analyzer (Micromeritics ASAP 2460, America) at 77 K in the relative pressure range of P/P_0. The specific surface area was determined by the Brunauer-Emmett-Teller (BET) method. The magnetic properties of the powders were measured by JDAW-2000C&D vibrating sample magnetometer (VSM). The morphologies of the powders were characterized by JEOL JSM-6490LV scanning electron microscope (SEM). Fourier Transform Infrared spectra (FTIR) were recorded using a Fourier transform infrared spectrometer (Thermo Scientific Nicolet iS50, America) over 4000-400 cm^{-1}. The samples were pressed into compact wafers using a stainless steel die under the pressure of 5 MPa for several minutes, a SL20QB contact angle meter was used to detect the contact angle using water as the droplet. Thermal images of the pellets were taken by an infrared thermal imaging camera (Fluke, apparatus model).

Sorption capacity test towards oil and organic solvents

Typically, 0.5 g dry carbon powders were added into a beaker filled with 20 g organic liquid without stirring. After 30 min, the soaked powders were magnetically collected, and the remaining oil in the beaker was weighed. The maximum oil sorption capacity of the powders was calculated by

$$q = \frac{20 - C_f}{0.5}$$

where q is the maximum sorption capacity ($g_{oil}/g_{sorbent}$), and C_f is the final weight of the oil.

Recycling test

After the oil-absorption test, the oil-containing superhydrophobic particles were magnetically removed from the mixtures and reused after three tetrahydrofuran rinses. Then, the clean powders were dried at 50 °C for the next oil-absorption cycle. The recyclability was evaluated by calculating the oil-absorption capacity of powders that experienced 20-cycles absorption. Also, the CA measurement was operated to evaluate the superhydrophobicity of reused powders.

Chemical stability tests

The chemical stability of magnetic powders was carried out in a series of solutions with pH in the range of 3-13 at room temperature. Firstly, 1 g powders were sprinkled into a beaker and mixed with 100 mL pre-made solution with a stable pH value. After 24 hours, the powders were recollected and dried. And then, the CA and adsorption capacity of powders were measured to determine pH stability. With the same method, a NaCl solution was prepared to imitate the seawater to investigate the stability of powders in a marine environment.

Results and discussion

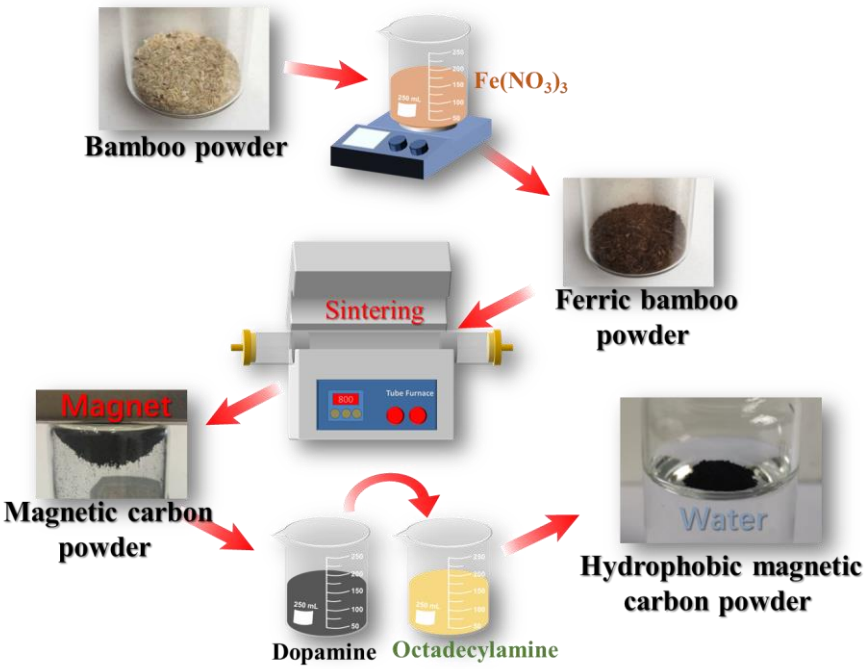

Fig. 1 Schematic diagram for the fabrication of hydrophobic magnetic carbon powder.

As illustrated in **Fig. 1**, the bamboo powder was used as a carbon precursor and was then mixed with $Fe(NO_3)_3$ solution. Magnetic particles were formed during the pyrolysis of the biomass-derived carbon. Additional bio-inspired surface modification conferred optimal hydrophobicity on the powders via grafting of long-chain alkane[37, 38].

The crystalline structure of the produced magnetic carbon powders was determined by XRD analysis. As shown In **Fig. 2a**, the XRD patterns of composite powders are manufactured with different ratios of basic materials. All three types of powders had distinctive face-centered cubic Fe_3O_4 (JCPDS NO.19-0629) peak shapes. When the $Fe(NO_3)_3$ ratio in raw materials increases, the peaks become sharper and more intense, indicating a higher Fe_3O_4 crystalline content. The presence of graphitized carbon also causes a significant peak near about 26.5°. XRD patterns were also employed to examine the impact of sintering temperatures on powder phase transitions. As shown in **Fig. 2b**, iron-containing crystalline phases, including Fe_3O_4 (JCPDS NO.19-0629), Fe_3C (JCPDS NO.35-0772), and Fe (JCPDS NO.06-0696), appeared. Specifically, for the C-2 fabricated at 600 ºC, recognizable Fe_3O_4 peaks together with graphite carbon could be seen. As the temperature rose to 700°C, the Fe peak became apparent, and the

Fe_3O_4 peaks faded in the curve of C-4. When the temperature reaches 800 °C, sharp Fe peaks, several Fe_3C peaks, and amorphous carbon peaks can be seen. Therefore, it can be inferred that the Fe-containing compounds were gradually reduced to elemental Fe with the increased sintering temperature. The BET test was subsequently used to determine the precise surface areas of the objects. In **Fig. 2c**, the nitrogen adsorption curves in C-2 and C-3 have attained saturation at low pressure. Due to micropores and mesopores, a characteristic type-IV isotherm was seen in C-1, C-4, and C-5[39]. As shown in **Table 2**, C-1, C-4, and C-5 had BET surface areas of 201.0, 186.2, and 178.3 m^2/g, respectively, which were more significant than the other two samples and advantageous for oil absorption. VSM evaluated the magnetic properties of the samples at room temperature due to the presence of Fe-containing components. The magnetic hysteresis curves of C-1, C-2, C-3, C-4, and C-5 revealed saturation magnetizations (Ms) of 3.8, 19.2, 101.1, 60.5, and 76.0 emu/g (**Fig. 2d**). The MPC magnetic hysteresis loops exhibited paramagnetic behavior between 20000 and -20000 Oe, devoid of remanence or coercivity. Magnetic saturation values of samples were also impacted by $Fe(NO_3)_3$/bamboo ratios and sintering temperatures. The paramagnetic characteristic and the ability to tailor the saturation values of the magnetic field significantly improved the operability of powder-like oil absorbers.

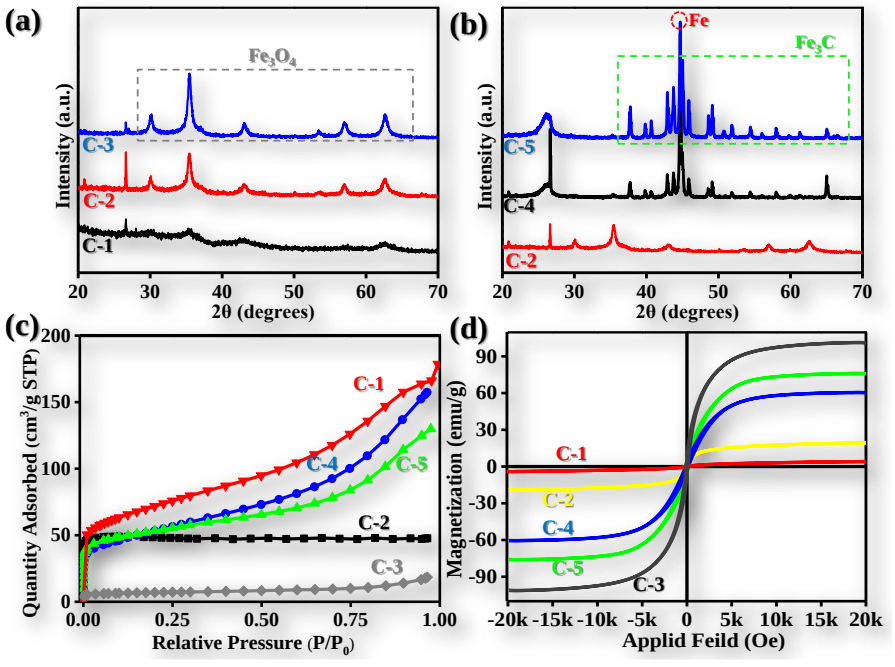

Fig. 2 XRD patterns of samples prepared at different ratios of raw materials (a) and prepared at different temperatures (b); Nitrogen adsorption-desorption isotherms (c) and Magnetization hysteresis loops of samples (d).

Table 2. Specific surface area and saturation magnetization of samples.

Sample	C-1	C-2	C-3	C-4	C-5
Specific surface area (m^2/g)	201.0	143.2	22.8	186.2	178.3
Saturation magnetization (emu/g)	3.8	19.2	101.1	60.6	76.0

Fig. 3a1-e1 illustrates the microstructures of MPCs. All MPCs had a honeycomb-like structure with cell diameters of 20–50 um at low magnification. Additionally, the magnified images (**Fig. 3a2-e2**) revealed the presence of numerous secondary pores in the cell wall, except for C-3, with sizes of roughly 1 um. After pyrolysis, the porous C-3 debris converted into uneven spheres due to the excess ferric salts. The photos in **Fig. 3a3-e3** provided further detail on the pore wall. We discovered that the walls of C-1 and C-2 were relatively smooth. While the walls of C-4 and C-5 were coated with a dense network of nanopores. Additionally, as illustrated in **Fig. 3c2**, the stratified microstructures of nanospheres in C-3 were revealed. C-4 and C-5 reflected hierarchical structures with honeycomb-like morphologies, including submillimeter-, micro-, and nanopores. The multilevel hierarchical structure was more conducive to oil storage and made it easier for oil to penetrate the interiors of MPCs. In comparison, C-1 and C-2 allow for the selection of only two types of pores.

The current work's target absorbents required a high absorption capacity and magnetic intensity. Both C-4 and C-5 had a desirable Ms value and a large specific surface area, which translated to a high absorption capacity and ease of use in oil spill remediation. Thus, considering the energy required for preparation and the functional properties, C-4 generated at 700 ^{o}C was chosen as the subject of the ensuing inquiry.

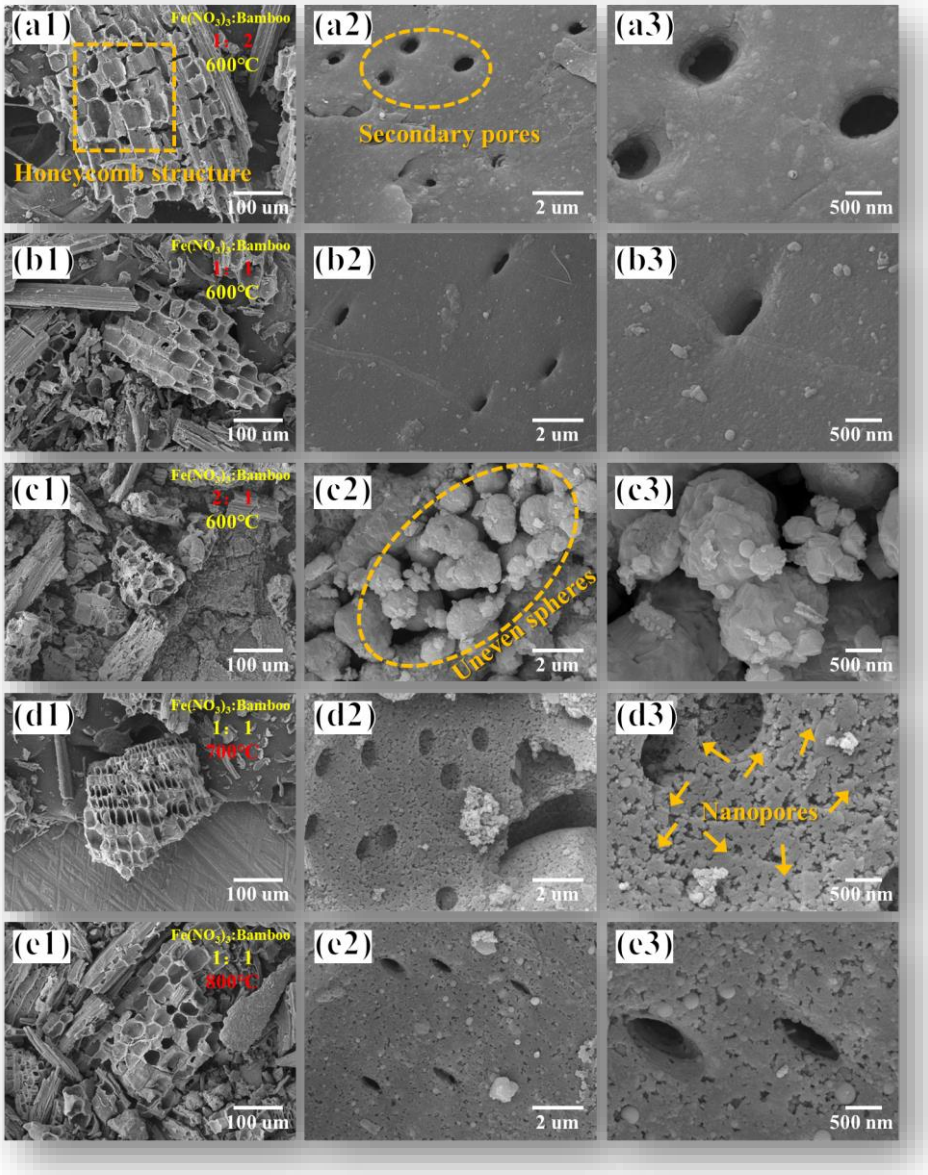

Fig. 3 SEM images of C-1 (a1-3), C-2 (b1-3), C-3 (c1-3), C-4 (d1-3) and C-5 (e1-3).

As mentioned before, MPCs' hydrophobicity and capacity to float are critical for oil spill remediation. However, due to their high density and hydrophilic surface, the MPCs in their prepared state cannot float stably over water. However, this problem could be solved by a bio-inspired surface grafting technique employed to endow the MPCs with hydrophobicity and avoid secondary contamination from absorbents. Through the typical Schiff base reaction and Michael addition caused by dopamine polymerization, ODA with a long alkyl chain was successfully grafted onto PDA-covered MPCs in this study. The detailed synthesis technique, as depicted in **Fig. 4**: Dopamine polymerization

first formed a PDA layer that shielded MPCs from corrosion and supplied functional groups as a site for grafting hydrophobic chemicals. After that, the ODA was covalently grafted onto MPCs-PDA via a standard Michael addition or Schiff base reaction between amino and quinone groups.

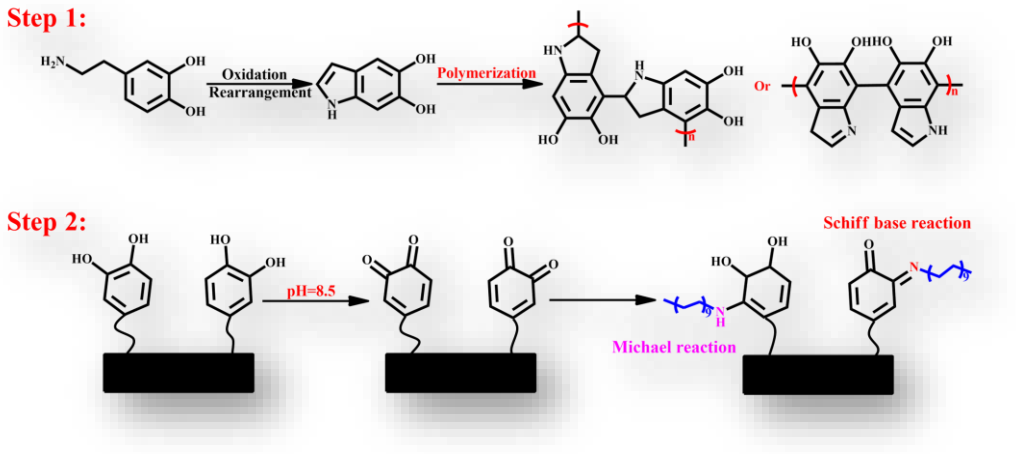

Fig. 4 Reaction mechanism of dopamine and ODA during the dip-coating process.

In order to compare the surface properties between the samples before and after coating, the FTIR spectra of pure MPCs and ODA-MPCs were compared in **Fig. 5a** to indicate MPCs' surface functionalization. The absorption peaks at approximately 1610 cm^{-1} (C=C stretching), 1485 cm^{-1} (N-H scissoring), and 1284 cm^{-1} (C-O stretching) prove that PDA was coated on the MPCs. The new peaks at 2915 and 2848 cm^{-1} on the ODA-MPCs curve were connected with CH stretching vibrations, which were contributed by the abundant methyl and methylene groups in ODA molecules. The peak at 1150 cm^{-1} might be attributable to the secondary amine's -C-N- stretching vibration, which provided the presence of an interaction between ODA and PDA. FTIR analysis confirms that ODA was successfully grafted onto the surface of MPCs.

MPCs were anticipated to be hydrophobic and float in water after the decoration of ODA. As a result, the clean MPCs and ODA-MPCs were dispersed into the sea surface independently. After 24 hours, nearly all pure MPCs sank to the bottom of the vial, whereas ODA-MPCs powders remained afloat on the water surface. The surface wetting test was used to determine the further hydrophilicity-to-hydrophobicity

transition. MPCs had a contact angle of approximately 0°, whereas ODA-MPCs had a contact angle of 135.5°. (**Fig. 5b**). Additionally, when an oil droplet was added to the unmodified MPCs, as demonstrated in **Fig. 5c**, the oil droplets were put to the MPCs and entirely repelled. In comparison, oil droplets could easily permeate ODA-MPCs due to their increased hydrophobicity. Based on the preceding, it can be concluded that ODA-coated MPCs exhibit superior water repellency, oil affinity, and floatability that can be used to address maritime oil spills.

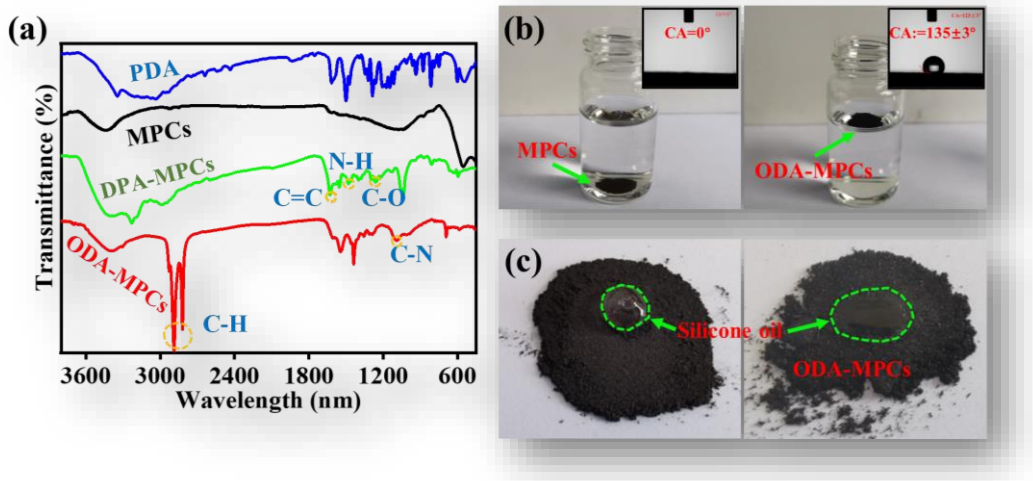

Fig. 5 FTIR spectra of PDA, MPCs, PDA-MPCs and ODA-MPCs (a); comparison of floatability (b) (inset: water contact angle); comparison of oil wettability (c).

Subsequently, the uptake capacity of ODA-MPCs was established. As shown in **Fig. 6a**, ODA-MPCs had a favorable sorption capability for various oils and nonpolar organic solvents, including high viscosity petroleum and silicone oils. Calculations indicate that the modified magnetic powders have absorption capacities ranging from 3.2 to 8.1 g/g. Due to the higher viscosity, the absorbed silicone oil (5000 cP•s) and petroleum can be successfully retained in hierarchically porous architectures of powders. We compare our work to many previously published powder-based oil sorbents using a literature search (**Table 3**) [21, 23, 40-42]. Although ODA-MPCs have a lower sorption capacity than other sorbents, their manufacture is simpler and less expensive. The raw materials are primarily constituted of biodegradable agricultural and forest byproducts.

Table 3. Comparison of powder sorbents reported in recent literature

materials	sorption capacity（g/g）	magnetic response	photothermal effect	references
fly ash composites	1.69	√	×	[40]
Fe_3O_4@C/Cu core-shell sub-micron materials	3.38	×	×	[21]
sawdust	3.59 to 7.83	√	×	[42]
silver nanocomposite	10.95 ± 0.47	×	×	[41]
hollow carbon microsphere	6.5 to 10.8	√	×	[23]
MPC	**3.2 to 8.1**	√	√	**This work**

Fig. 6b illustrates the absorption capability of ODA-MPCs after they have been subjected to a 20-cycles absorption experiment. In comparison to the data in **Fig. 6a**, the change in either sorption capacity or the water contact angles was negligible for the high-viscosity silicone oil, n-hexane, and petroleum, indicating improved cycling performances of ODA-MPCs. The absorbent used in practice must be able to survive in acidic, alkaline, and hypersaline environments, which are prevalent in the marine environment. Thus, the absorption capacity and contact angles of ODA-MPCs were measured after 24 hours of immersion in 3 percent salty water with varying pH values. As shown in **Fig. 6c**, the absorption capacity of ODA-MPCs for crude oil remained constant at approximately 6.2 g/g under diverse circumstances. Additionally, the contact angle values vary somewhat between 132°and 134°. These findings suggested that ODA-MPCs can reserve their capacity for surface wetting and oil absorption into the ocean.

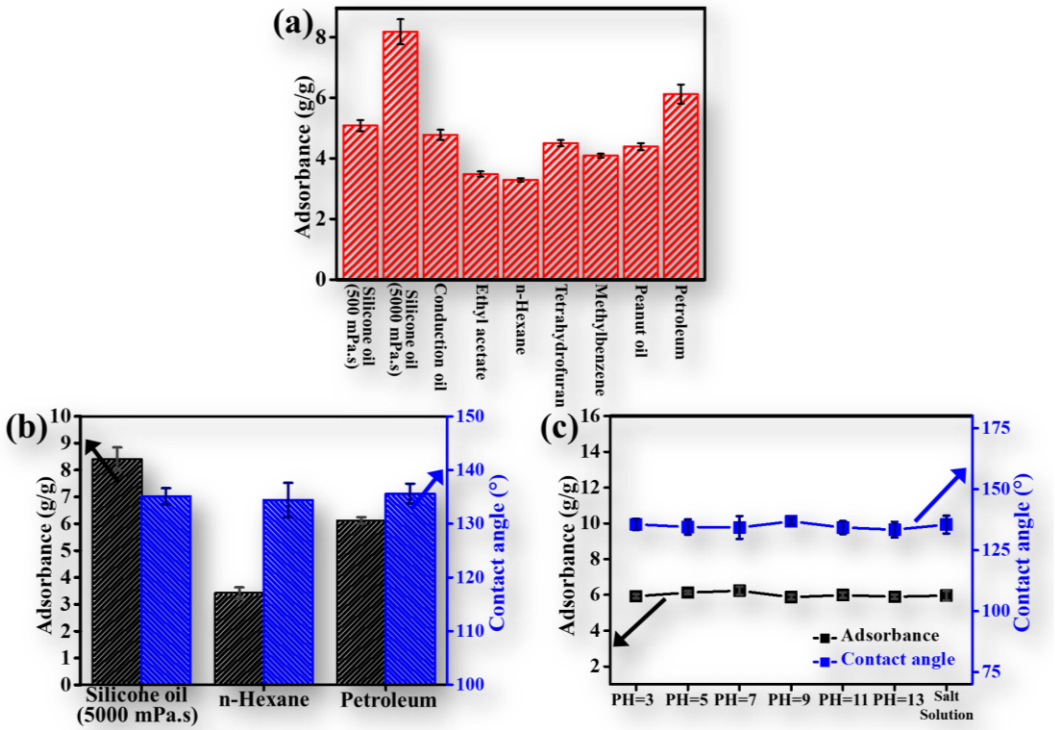

285

286 **Fig. 6** (a) Absorption capacity of the ODA-MPCs for different oils and solvents; (b)
287 Effect of pH value on the oil-absorption capacity and contact angles of the hydrophobic
288 ODA-MPCs; (c) Absorption capacities towards different oils and organic solvents after
289 20 cycles of usage and remanent contact angle.

290 **Fig. 7a** presents the processes of removing crude oil from the water by ODA-MPCs
291 under an external magnetic field. When the powers were cast to an oil layer floating on
292 the water surface, the crude oil gradually accumulated around the powders and was
293 absorbed within 60 s. The absorption-saturated particles were drawn out of the water
294 by a magnetic column due to the introduction of magnetic compounds, thereby
295 releasing clean water. The above test supports the applicability of MPCs under practical
296 marine conditions. Concerning the oil/water separation process, the hydrophobicity and
297 lipophilicity of ODA-MPCs were related to the grafted long-chain alkane and rough
298 surface on substrates, in accordance with the theory of wettability on the solid surface.
299 [43]. The introduced alkane chains decreased the surface tension, limiting the wetting
300 of water droplets. Generally, the influence of surface roughness on wettability could be
301 explained by Wenzel and Cassie's model. For ODA-MPCs, the air bubbles trapped on

the rough surface also drastically reduced the contact area of water with the substrates and led to the hydrophobic performance described by the traditional Cassie model:

$$\cos\theta r = \varphi\cos\theta e + \varphi - 1$$

where θr is the water CA on the rough surface, θe is the equilibrium water CA on the smooth surface, and φ is the fraction of the drop footprint area in contact with the solid (the solid fraction) ($\varphi < 1$).

Unlike water droplets, the wetting performance was dramatically enhanced, and the true contact angle was significantly enlarged when the substrate of ODA-MPCs suffered from the oils. The Wenzel model could explain this phenomenon:

$$\cos\theta r = \frac{1}{f}\cos\theta e$$

Where θr is the oil CA on the rough surface, θe is the equilibrium oil CA on the smooth surface, and f is the roughness factor, defined as the ratio of the actual area of the rough surface to the geometric projected area ($f > 1$). It could be predicted that the long chains are aggregated to build a thin layer of hydrophobic film to repulse water while they can be well stretched to form a transitional layer in the oil droplets (**Fig.7b**). Therefore, the modified MPCs exhibit desirable hydrophobicity and lipophilicity.

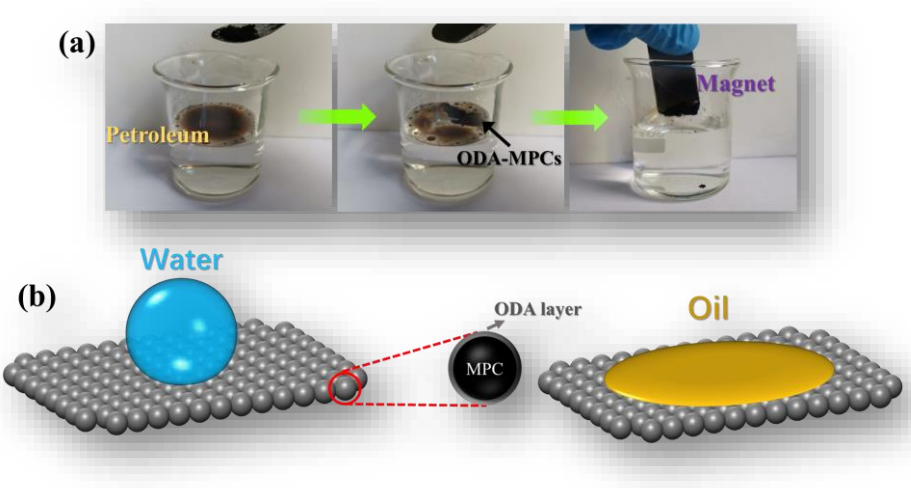

Fig. 7 Removal of petroleum from water surface by ODA-MPCs with a magnetic field (a); schematic illustration for wettability of ODA-MPCs (b).

Compared to common organic solvents, oils with high viscosity diffuse slowly due to

their low fluidity. However, the rheology properties of the oil are temperature-dependent. Thus, employing a photothermal approach to achieve efficient oil recovery provides several specific advantages in a marine environment. Due to their broad-spectrum solar light absorption, carbon-based materials are an excellent photothermal absorbent for the fast adsorption of high-viscosity oil. **Fig. 8a** showed thermal infrared pictures of ODA-MPCs demonstrating the normal photothermal effect. When exposed to sunlight, powders reach an equilibrium temperature of 62 °C in a matter of seconds, but without sunlight, they reach a temperature of roughly 38 °C (in summer). A difference of 24 °C in temperature notably influences the viscosity of high-viscosity oil. To demonstrate the effect, we studied the spreading behavior of oil droplets on ODA-MPCs. The evolution of the droplet's diameter with different exposure durations is recorded by the thermal infrared images in **Fig.8b**. Under sunlight, it took 22 seconds for the diameter of the oil droplet to double and just 63 seconds for it to reach its maximum diameter. However, in the absence of direct sunlight, the diameter of the oil droplet spreads to twice its initial diameter in 41 seconds and achieves its maximum diameter in 105 seconds. The different spread speeds of the oil droplets with and without sunlight exposure indicated that the increased temperature caused by sunlight might promote the fluidity and diffusion of heavy crude oil, which consequently facilitates the adsorption of high-viscosity oil. In **Fig.8c,** a schematic representation of the photothermal effect being activated in magnetic porous biochar to reduce the viscosity of oils was shown. Due to their low fluidity, the powder-like MPCs are typically difficult to spread into such thick fluids. When exposed to the sun, the generated heat significantly reduces the viscosity of the oil, boosting powder dispersion and absorption efficiency.

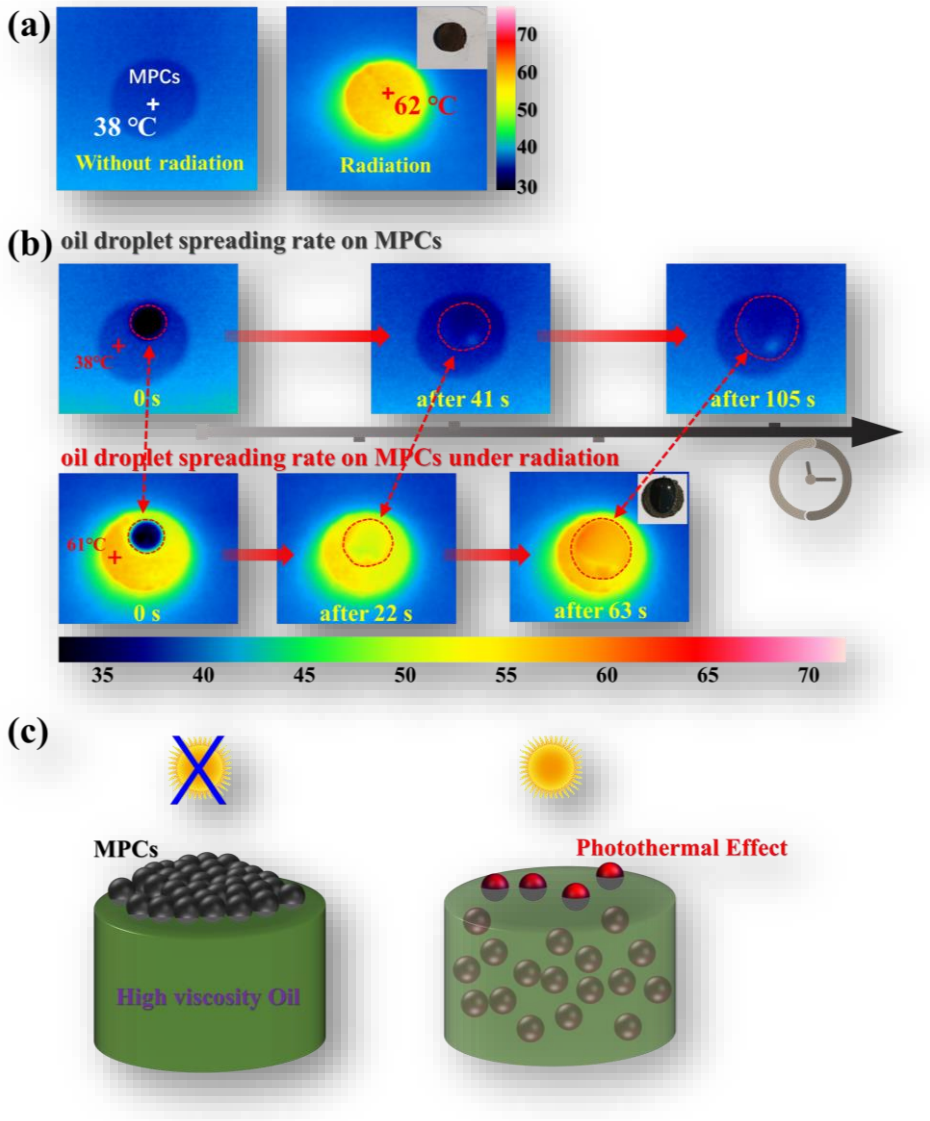

Fig 8. Infrared images: comparison of temperature in MPCs without solar radiation and under solar radiation (a); time-dependent the spreading rate of an oil droplet on surface MPCs without solar radiation and under solar radiation (b). schematic illustration of solar-heated ODA-MPCs for the fast adsorption of high viscosity oil (c).

Conclusions

In this study, we produced porous carbon powders with hydrophobicity, photothermal conversion capacity, and magnetic responsiveness for use in crude oil spill recovery. The essential components were inexpensive and ecologically sustainable bamboo powder. By altering the powders modified with ODA, the crude oil absorption capacity increased to greater than 6.2 g/g. Meanwhile, the powders produced could be utilized

in acidic, alkaline, and hypersaline settings. In addition, by applying the magnetic field, the porous carbon particles could be localized in the oil-water region for sorption and recovery. In addition, by leveraging the photothermal effect, the area surrounding the powders became much hotter when exposed to sunshine, facilitating the efficient absorption of high-viscosity oil. As a result, we expect that this form of carbon powder will be widely utilized in crude oil spills.

This work is supported by the National Natural Science Foundation of China with grant number 52002403 and 51703248.

References

[1] G.L. Cao, Y.G. Wang, C.Y. Wang, S.H. Ho, A dually prewetted membrane for continuous filtration of water-in-light oil, oil-in-water, and water-in-heavy oil multiphase emulsion mixtures, J. Mater. Chem. A 7 (2019) 11305-11313.

[2] W. Chen, P.C. Zhang, R.H. Zang, J.B. Fan, S.T. Wang, B.L. Wang, J.X. Meng, Nacre-Inspired Mineralized Films with High Transparency and Mechanically Robust Underwater Superoleophobicity, Adv. Mater. 32 (2020) 1907413.

[3] X.Q. Cheng, Z.K. Sun, X.B. Yang, Z.X. Li, Y.J. Zhang, P. Wang, H. Liang, J. Ma, L. Shao, Construction of superhydrophilic hierarchical polyacrylonitrile nanofiber membranes by in situ asymmetry engineering for unprecedently ultrafast oil-water emulsion separation, J. Mater. Chem. A 8 (2020) 16933-16942.

[4] X. Ge, W.X. Qin, H.M. Zhang, G.Z. Wang, Y.X. Zhang, C.Z. Yu, A three-dimensional porous Co@C/carbon foam hybrid monolith for exceptional oil-water separation, Nanoscale 11 (2019) 12161-12168.

[5] M.B. Wu, S. Huang, T.Y. Liu, J. Wu, S. Agarwal, A. Greiner, Z.K. Xu, Compressible Carbon Sponges from Delignified Wood for Fast Cleanup and Enhanced Recovery of Crude Oil Spills by Joule Heat and Photothermal Effect, Adv. Funct. Mater. 31 (2021) 2006806.

[6] A. Farinmade, O.F. Ojo, J. Trout, J.B. He, V. John, D.A. Blake, Y.M. Lvov, D.H. Zhang, D. Nguyen, A. Bose, Targeted and Stimulus-Responsive Delivery of Surfactant to the Oil-Water Interface for Applications in Oil Spill Remediation, ACS Appl. Mater. Inter. 12 (2020) 1840-1849.

[7] D. Motorin, H. Roozbahani, H. Handroos, Development of a novel method for estimating and planning automatic skimmer operation in response to offshore oil spills, J. Environ. Manage. (2022) 115451.

[8] L. G. Faksness, F. Leirvik, I.C. Taban, F. Engen, H.V. Jensen, J.W. Holbu, H. Dolva, M. Bratveit, Offshore field experiments with in-situ burning of oil: Emissions and burn efficiency, Environ. Res. 205 (2022) 112419.

[9] M. Omarova, L.T. Swientoniewski, I.K.M. Tsengam, D.A. Blake, V. John, A. McCormick, G.D. Bothun, S.R. Raghavan, A. Bose, Biofilm Formation by Hydrocarbon-Degrading Marine Bacteria and Its Effects on Oil Dispersion, ACS. Sustain. Chem. Eng. 7 (2019) 14490-14499.

[10] S.H. Wu, H.C. Yang, G.P. Xiong, Y.K. Tian, B.Y. Gong, T.F. Luo, T.S. Fisher, J.H. Yan, K.F. Cen, Z. Bo, K.K. Ostrikov, Spill-SOS: Self-Pumping Siphon-Capillary Oil Recovery, ACS Nano 13 (2019) 13027-13036.

[11] L. Oliveira, J. Saleem, A. Bazargan, J.L.D. Duarte, G. McKay, L. Meili, Sorption as a rapidly response for oil spill accidents: A material and mechanistic approach, J. Hazard. Mater. 407 (2021) 124842.

[12] J.F. Xu, R. Cao, M.S. Li, G.X. Chen, J.F. Tian, Superhydrophobic and superoleophilic cuttlebone with an inherent lamellar structure for continuous and effective oil spill cleanup, Chem. Eng. J. 420 (2021) 127596.

[13] H.Y. Yu, M. Wu, G.G. Duan, X. Gong, One-step fabrication of eco-friendly superhydrophobic fabrics for high-efficiency oil/water separation and oil spill cleanup, Nanoscale 14 (2022) 1296-1309.

411 [14] Z. Guo, B. Long, S. Gao, J. Luo, L. Wang, X. Huang, D. Wang, H. Xue, J. Gao,
412 Carbon nanofiber based superhydrophobic foam composite for high performance
413 oil/water separation, J. Hazard. Mater. 402 (2021) 123838.
414 [15] P.K. Renjith, C. Sarathchandran, V.S. Achary, N. Chandramohanakumar, V. Sekkar,
415 Micro-cellular polymer foam supported silica aerogel: Eco-friendly tool for petroleum
416 oil spill cleanup, J. Hazard. Mater. 415 (2021) 125548.
417 [16] L. Jin, Y. Gao, Y. Huang, M. Ou, Z. Liu, X. Zhang, C. He, B. Su, W. Zhao, C. Zhao,
418 Mussel-Inspired and In Situ Polymerization-Modified Commercial Sponge for
419 Efficient Crude Oil and Organic Solvent Adsorption, ACS Appl. Mater. Inter. 14(2)
420 (2022) 2663-2673.
421 [17] H. Kim, G. Zhang, M. Wu, J.S. Guo, C. Nam, Highly efficient and recyclable
422 polyolefin-based magnetic sorbent for oils and organic solvents spill cleanup, J. Hazard.
423 Mater. 419 (2021) 126485.
424 [18] M. Yang, B. Chen, X.Y. Xin, X. Song, J.B. Liu, G.H. Dong, K. Lee, B.Y. Zhang,
425 Interactions between microplastics and oil dispersion in the marine environment, J.
426 Hazard. Mater. 403 (2021) 123944.
427 [19] Z.K. Chen, C.J. An, M. Boufadel, E. Owens, Z. Chen, K. Lee, Y.T. Cao, M.F. Cai,
428 Use of surface-washing agents for the treatment of oiled shorelines: Research
429 advancements, technical applications and future challenges, Chem. Eng. J. 391 (2020)
430 123565.
431 [20] Q. Feng, C.J. An, Z. Chen, E. Owens, H.B. Niu, Z. Wang, Assessing the coastal
432 sensitivity to oil spills from the perspective of ecosystem services: A case study for
433 Canada's pacific coast, J Environ. Manage. 296 (2021) 113240.
434 [21] T.Q. Liu, Z.J. Li, G.M. Shi, Q. Zhao, X. Chen, X.L. Chen, Y.L. Li, Facile
435 preparation of Fe_3O_4@C/Cu core-shell sub-micron materials for oil removal from water
436 surface, Appl. Surf. Sci. 466 (2019) 483-489.

437 [22] P.M. Reddy, C.J. Chang, J.K. Chen, M.T. Wu, C.F. Wang, Robust polymer grafted
438 Fe3O4 nanospheres for benign removal of oil from water, Appl. Surf. Sci. 368 (2016)
439 27-35.
440 [23] N. Yang, Z.-X. Luo, S.-C. Chen, G. Wu, Y.-Z. Wang, Superhydrophobic magnetic
441 hollow carbon microspheres with hierarchical micro/nano- structure for ultrafast and
442 highly-efficient multitasking oil-water separation, Carbon 174 (2021) 70-78.
443 [24] S. Singh, R. Jelinek, Solar-mediated oil-spill cleanup by a carbon dot-polyurethane
444 sponge, Carbon 160 (2020) 196-203.
445 [25] J. Ge, L.-A. Shi, Y.-C. Wang, H.-Y. Zhao, H.-B. Yao, Y.-B. Zhu, Y. Zhang, H.-W.
446 Zhu, H.-A. Wu, S.-H. Yu, Joule-heated graphene-wrapped sponge enables fast cleanup
447 of viscous crude-oil spill, Nat.Nanotechnol. 12 (2017) 434-440.
448 [26] Y.H. Song, L.A. Shi, H.Y. Xing, K. Jiang, J. Ge, L. Dong, Y. Lu, S.H. Yu, A
449 Magneto-Heated Ferrimagnetic Sponge for Continuous Recovery of Viscous Crude Oil,
450 Adv. Mater. 33 (2021) 2100074.
451 [27] C. Gong, J.C. Lao, B.Y. Wang, X.Y. Li, G.J. Li, J. Gao, Y.Z. Wan, X.H. Sun, R.S.
452 Guo, J.Y. Luo, Fast and all-weather cleanup of viscous crude-oil spills with MXene
453 wrapped sponge, J. Mater. Chem. A 8 (2020) 20162-20167.
454 [28] Q. Li, Q. Sun, Y. Li, T. Wu, S. Li, H. Zhang, F. Huang, Solar-Heating Crassula
455 perforata-Structured Superoleophilic CuO@CuS/PDMS Nanowire Arrays on Copper
456 Foam for Fast Remediation of Viscous Crude Oil Spill, ACS Appl. Mater. Inter. 12
457 (2020) 19476-19482.
458 [29] X.Z. Ma, C. Zhang, P. Gnanasekar, P. Xiao, Q. Luo, S.Q. Li, D.D. Qin, T. Chen, J.
459 Chen, J. Zhu, N. Yan, Mechanically robust, solar-driven, and degradable lignin-based
460 polyurethane adsorbent for efficient crude oil spill remediation, Chem. Eng. J. 415
461 (2021) 128956.
462 [30] X.Z. Jin, X.D. Qi, Y. Wang, J.H. Yang, H. Li, Z.W. Zhou, Y. Wang,
463 Polypyrrole/Helical Carbon Nanotube Composite with Marvelous Photothermoelectric

Performance for Longevous and Intelligent Internet of Things Application, ACS Appl. Mater. Inter. 13(7) (2021) 8808-8822.
[31] Z. Li, Z. Lin, M. Han, Y. Mu, P. Yu, Y. Zhang, J. Yu, Flexible electrospun carbon nanofibers/silicone composite films for electromagnetic interference shielding, electrothermal and photothermal applications, Chem. Eng. J. 420 (2021) 129826.
33[32] Y. Zhao, T. Zhao, Y. Cao, J. Sun, Q. Zhou, H. Chen, S. Guo, Y. Wang, Y. Zhen, X.-J. Liang, S. Zhang, Temperature-Sensitive Lipid-Coated Carbon Nanotubes for Synergistic Photothermal Therapy and Gene Therapy, ACS Nano 15(4) (2021) 6517-6529.
[33] Y. Wu, H. Huang, W. Zhou, C. You, H. Ye, J. Chen, S. Zang, J. Yun, X. Chen, L. Wang, Z. Yuan, High-Porosity Lamellar Films Prepared by a Multistage Assembly Strategy for Efficient Photothermal Water Evaporation and Power Generation, ACS Appl. Mater. Inter. 14(25) (2022) 29099-29110.
[34] Z. Liu, M. Chen, C. Lin, F. Li, J.T. Aladejana, J. Hong, G. Zhao, Z. Qin, X. Zhu, W. Zhang, D. Chen, X. Peng, T. Chen, Solar-assisted high-efficient cleanup of viscous crude oil spill using an ink-modified plant fiber sponge, J. Hazard. Mater. 432 (2022) 128740.
[35] S. Wu, D. Chen, G. Zhao, Y. Cheng, B. Sun, X. Yan, W. Han, G. Chen, X. Zhang, Controllable synthesis of a robust sucrose-derived bio-carbon foam with 3D hierarchical porous structure for thermal insulation, flame retardancy and oil absorption, Chem. Eng. J. 434 (2022) 134514.
[36] Y. Yue, Y. Wang, J. Li, W. Cheng, G. Han, T. Lu, C. Huang, Q. Wu, J. Jiang, High strength and ultralight lignin-mediated fire-resistant aerogel for repeated oil/water separation, Carbon 193 (2022) 285-297.
[37] S. Chen, Y. Cao, J. Feng, Polydopamine As an Efficient and Robust Platform to Functionalize Carbon Fiber for High-Performance Polymer Composites, ACS Appl. Mater. Inter. 6 (2014) 349-356.

[38] L. Luo, X. Chen, Y. Wang, J. Yue, Z. Du, X. Huang, X.-Z. Tang, Bio-inspired modification of silicon carbide foams for oil/water separation and rapid power-free absorption towards highly viscous oils, Ceram. Int. 44 (2018) 12021-12029.

[39] G. Zeng, X. Li, Y. Wei, T. Guo, X. Huang, X. Chen, X.-Z. Tang, Significantly toughened SiC foams with enhanced microwave absorption via in situ growth of Si_3N_4 nanowires, Chem. Eng. J. 426 (2021) 131745.

[40] L. Bandura, R. Panek, J. Madej, W. Franus, Synthesis of zeolite-carbon composites using high-carbon fly ash and their adsorption abilities towards petroleum substances, Fuel 283 (2021) 119173.

[41] M.A. Ali, S.A. Shaaban-Dessuuki, N.A. El-Wassefy, S.I. Mostafa, M.H. Hussein, Adsorption of crude and waste diesel oil onto agar-carboxymethylcellulose-silver nanocomposite in aqueous media, Inorg. Chem. Commun. 133 (2021) 108915.

[42] Z. Yin, Y. Li, T. Song, M. Bao, Y. Li, J. Lu, Y. Li, Preparation of superhydrophobic magnetic sawdust for effective oil/water separation, J. Clean. Prod. 253 (2020) 120058.

[43] B. Wang, W. Liang, Z. Guo, W. Liu, Biomimetic super-lyophobic and super-lyophilic materials applied for oil/water separation: a new strategy beyond nature, Chem. Soc. Rev. 44 (2015) 336-361.